Advances in Applied Energy 18 (2025) 100221

Contents lists available at ScienceDirect

Advances in Applied Energy

journal homepage: www.elsevier.com/locate/adapen

Global sensitivity analysis towards non-invasive parameterization of the electrochemical-thermal model for lithium-ion batteries

Jue Chen [a,b,c,*,1], Sven Patrick Mattus [a,b,c,1], Wenjiong Cao [a,b,c], Dirk Uwe Sauer [a,b,c,d], Weihan Li [a,b,c,*]

[a] Center for Aging, Reliability and Lifetime Prediction of Electrochemical and Power Electronic Systems (CARL), RWTH Aachen University, Campus-Boulevard 89, 52074 Aachen, Germany
[b] Institute for Power Electronics and Electrical Drives (ISEA), RWTH Aachen University, Campus-Boulevard 89, 52074 Aachen, Germany
[c] Juelich Aachen Research Alliance, JARA-Energy, Templergraben 55, Aachen, 52056, Germany
[d] Helmholtz Institute Muenster (HI MS), IMD-4, Forschungszentrum Juelich, Germany

ARTICLE INFO

Keywords:
Lithium-ion battery
Electrochemical-thermal model
Sensitivity
Non-invasive
Parameterization

ABSTRACT

High-fidelity electrochemical-thermal models are essential for performance improvement, charge/discharge strategy optimization, and the safe operation of lithium-ion batteries. However, model performance significantly relies on the accuracy of parameters, whose measurement is limited by laboratory conditions. Non-invasive methods based on relatively accessible current, voltage, and temperature data combined with artificial intelligence are promising for rapid parameterization of battery models. However, the model's complexity and the data's poor quality increase the difficulty of applying the methodology. To design a reasonable identification framework and obtain reliable data, the identifiability of model parameters must be analyzed under different operating conditions. This paper develops an identifiability analysis framework to investigate the impact of model parameters on voltage and temperature outputs and the impact of key operating variables, i.e., current rate and ambient temperature. By adjusting operating conditions, the sensitivity of specific parameters can be improved by two orders of magnitude. The results are discussed in detail concerning the model modeling mechanism and the physical meaning of the parameters, with a focus on improving non-invasive parameterization in terms of experimental design and identification strategy.

1. Introduction

Lithium-ion batteries (LIBs) dominate the electrical energy storage market and are widely used in both stationary and automotive applications due to their high energy density, low self-discharge, and long lifespan [1]. However, the performance and lifetime of LIBs are affected by operating conditions, where the temperature plays a crucial role. In particular, the challenges posed by thermal safety issues have created an urgent need for an effective thermal management system for batteries [2,3]. A well-performing thermal management system requires accurate models to simulate battery behavior and cost-effective parameterization methods for these models [4].

To model the electrical and thermal behaviors of LIBs, equivalent circuit models and electrochemical models are two widely used models. The former uses circuit components to simulate the electrical characteristics of the batteries, which has a simple structure and low computational cost [5]. The parameters of these models can be updated using online identification methods to simulate the voltage and estimate the state of LIBs accurately [6,7]. Furthermore, different electro-thermal models have been developed for the thermal predictions [8]. However, the parameters of such models usually lack a strong physical meaning and therefore face challenges such as low interpolation ability. The latter, by contrast, is based on the porous electrode and concentrated solution theory, which is therefore capable of presenting internal physical states, such as lithium-ion concentrations and potentials, enabling high interpretability [9]. To further model the thermal behavior of LIBs, both models can be coupled with a thermal model to simulate the temperature change due to heat generation and dissipation during the charging and discharging process of the battery. Due to its high interpolation and extrapolation ability, the electrochemical-thermal model (ECTM) is becoming more

* Corresponding authors at: Center for Aging, Reliability and Lifetime Prediction of Electrochemical and Power Electronic Systems (CARL), RWTH Aachen University, Campus-Boulevard 89, 52074 Aachen, Germany.
E-mail addresses: jue.chen@isea.rwth-aachen.de (J. Chen), weihan.li@isea.rwth-aachen.de (W. Li).
[1] These authors contributed equally to this work.

https://doi.org/10.1016/j.adapen.2025.100221
Received 28 February 2025; Received in revised form 29 April 2025; Accepted 29 April 2025
Available online 15 May 2025

Nomenclature

A_{area}	Electrode surface area
a	Interfacial area of spherical particles
c_e	Electrolyte Li-ion concentration
c_s	Electrode Li-ion concentration
c_{ss}	Electrode surface concentration
$c^+_{s,max}$	Maximum ionic concentration
$C_{p,i}$	Specific heat capacity
D_e	Electrolyte diffusion coefficient
D_s	Solid diffusion coefficient
$E_{A,X}$	Activation energy
F	Faraday constant
h_{cell}	Equivalent heat exchange coefficient
i_0	Exchange current density
k	Reaction rate
L	Length of the domain
X	Cell parameter
Q_{ohm}	Ohmic heat
Q_{rxn}	Irreversible heat
Q_{rev}	Reversible heat
Q_{tot}	Total heat
R	Universal gas constant
R_p	Particle radius
R_{SEI}	SEI film resistance
SI	Sensitivity index
T	Cell temperature
T_{ref}	Reference temperature
T_{amb}	Ambient temperature
U	Open circuit voltage
V	Terminal voltage
$V(\cdot)$	Variance
Y	Model output
σ_s	Electrode conductivity
σ_e	Electrolyte conductivity
κ_{eff}	Effective electrolyte conductivity
σ_{eff}	Effective electrode conductivity
ϕ_s	Solid-phase potential
ϕ_e	Electrolyte potential
t^0_+	Transference number of lithium cation
ρ_i	Volumetric mass density
λ_i	Thermal conductivity
ε_s	Active material volume fraction
ε_e	Electrolyte volume fraction
η	Overpotential of intercalation
θ_p	Cathode lithiation
θ_n	Anode lithiation

List of abbreviation

$ECTM$	Electrochemical-thermal model
LIB	Lithium-ion battery
OAT	One-at-A-Time
DOD	Depth of discharge
GSA	Global sensitivity analysis
SEI	Solid electrolyte interphase
$P2D$	Pseudo-Two-Dimensional
DFN	Doyle–Fuller–Newman
NMC	Nickel manganese cobalt oxide
QMC	Quasi-Monte Carlo
OCV	Open circuit voltage
MC	Monte-Carlo
BCI	Bootstrap confidence intervals
$RMSE$	Root mean square error
$C-rate$	Current rate
SI	Sobol index

and more popular in understanding and managing the electrical and thermal behaviors of LIBs. However, the performance of ECTMs relies heavily on precise parameters, and rapid and accurate parameterization of ECTMs remains a challenge. State-of-the-art parameterization approaches usually require opening the battery cell in the glove boxes and measuring the physical parameters of each component. Such invasive methods are limited by complex laboratory conditions, expensive measurement devices, and time-consuming procedures. Moreover, the batteries cannot be used anymore after the invasive measurement [10,11]. In contrast, non-invasive approaches use easily accessible data, e.g., current, voltage, and surface temperature, and optimization algorithms to parameterize the electrochemical models [12]. However, the primary challenge for such data-driven parameterization approaches is the significant differences in the identification ability of the parameters due to the high complexity and nonlinearity of the electrochemical model.

To understand the identification abilities of the physical parameters, sensitivity analysis has been widely investigated for LIBs: By analyzing the sensitivity of measurable states of LIBs on the value changes of the physical parameters, we are able to understand how these parameters affect the model behavior and what the mechanism behind it is. Sensitivity analysis methods can generally be divided into local methods, which analyze the sensitivity around the reference value, and global methods, which analyze the sensitivity of the entire parameter value space.

Park et al. [13] derived a sensitivity matrix of electrochemical parameters using first-order partial derivatives and integrated this approach into a parameter identification framework for the Newman model via Fisher information. A drawback of this method is that its implementation is highly demanding, as the analytical derivation of the sensitivity matrix for battery models is exceedingly complex. In contrast, the One-at-A-Time (OAT) method, where only one parameter is varied within its boundaries while others remain fixed at their nominal value, is easier to implement [14]. Li et al. analyzed the sensitivity of 26 parameters for an electrochemical model at different current rates (C-rates) and depth of discharge (DOD) ranges under real-world driving conditions of electric vehicles using the OAT method [15]. Similarly, Song et al. extended the application of the OAT method to analyze the sensitivities of the parameters of an ECTM, focusing on the heat generation rate [16]. Although less computationally intensive, local sensitivity analysis methods examine only a small portion of the value space around the nominal values [17].

In contrast, global sensitivity analysis (GSA) involves simultaneously varying several or all model parameters, enabling a comprehensive exploration of the parameter value space and assessing parameter sensitivity in a “global sense” [18]. Appiah et al. conducted a sensitivity analysis of a battery degradation model by training a differentiable surrogate Gaussian regression process model using various randomly sampled parameter sets [19]. The effect of model parameters on the thickness of the solid electrolyte interphase (SEI) and irreversible charge loss was thus obtained. However, this method requires constructing a high-quality regression model in advance, making preparatory work complex and time-consuming. The Morris method, also known as the Elementary Effect Test, is commonly used in global

sensitivity analysis for various LIB models [20,21]. This method reduces the number of model calculations through a specific sampling strategy, employing two statistical indices to represent the effect of a parameter on the output and its interaction with other parameters. Deng et al. performed a sensitivity analysis of physics-based model parameters for solid-state batteries using the Morris method [21]. However, the Morris method does not provide information about the intensity of interactions between parameters [22], which is crucial for developing an accurate and efficient parameterization framework for the battery model.

To comprehensively analyze the sensitivity of parameters and their interactions with a given parameter value space, the Sobol method, which can dissect the total variance of the model output into contributions from individual parameters and their interactions, has drawn significant attention. Lin et al. employed the Sobol method to analyze the impact of 46 parameters on discharge capacity and temperature variation in a 3D multiphysics model, identifying nine parameters with notable sensitivity and strong interactions among them [23]. Streb et al. applied the Sobol method to optimize experimental design, thereby enhancing parameter estimation [24]. Furthermore, the Sobol method plays an important role in identifying the impedance spectrum of LIBs [25]. Although the Sobol method has been widely applied to various battery models, a comprehensive analysis of the identifiability of ECTM parameters with respect to terminal voltage and battery temperature is still lacking. Additionally, the influence of operating conditions, including ambient temperature and current rate, on the sensitivity of these parameters has yet to be thoroughly investigated. Such insights are essential for the non-invasive parameterization of ECTMs for LIBs.

This study aims to address existing research gaps by analyzing, for the first time, the identifiability of 39 parameters of the ECTM with respect to voltage and temperature outputs across the entire value space using the Sobol method. First, an electrochemical-thermal coupling model is developed, whose parameters were benchmarked through a literature review and experiments. Full-order and first-order Sobol sensitivity indices were computed and used to rank the identifiability of the parameters, identifying the key parameters affecting the voltage and temperature outputs of the model. Additionally, second-order Sobol indices were analyzed to reveal interactions between specific parameters. To further explore the impact of significant operating factors on parameter identifiability, Sobol indices were computed under nine distinct operating conditions, each characterized by variations in ambient temperature and discharge current rates. The results were then interpreted in the context of the ECTM's underlying modeling mechanisms, providing a physical explanation for the observed changes in parameter sensitivity. Finally, a Pareto ranking method was applied to rank and group the parameters according to their sensitivity and importance.

2. Battery modeling

The methodology developed in this work can be implemented on LIB models across various platforms, including COMSOL, Python, C++, and MATLAB. For result visualization, we selected LIONSIMBA, an open-access ECTM for LIBs in MATLAB [26]. LIONSIMBA is based on the Pseudo-Two-Dimensional (P2D) model, which is numerically solved using a finite-volume method. The P2D model, or Doyle–Fuller–Newman (DFN) model, is a widely recognized and widely used electrochemical model for LIBs in the literature. Fig. 1 illustrates the working principles of the ECTM, which is described in detail in Sections 2.1 and 2.2.

2.1. Electrochemical model

The P2D model for LIBs assumes porous electrodes and encompasses the dynamics of both solid and electrolyte components, alongside the transport phenomena of lithium ions within the spatial and temporal domains of the LIB cell. This model enables the derivation of internal states, such as lithium concentrations and potentials within the cells [9]. In the P2D model, only the dynamics along the thickness direction of the electrode are considered, while it is assumed that the dynamics along the other two directions are unaffected by chemical reaction kinetics. The battery's behavior is described by a set of coupled, nonlinear partial differential–algebraic equations and their associated boundary conditions [26], which are summarized in Table S1 and S2 in the supplementary material of this work.

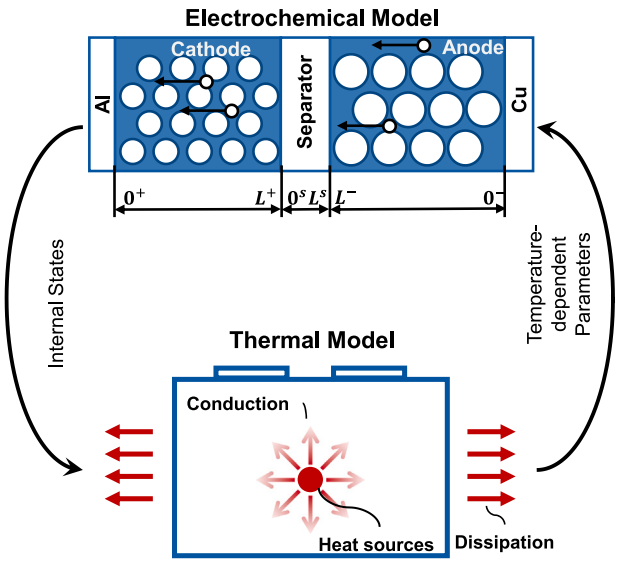

Fig. 1. Illustration of the coupling of the ECTM. The thermal model calculates the heat source from the internal states of the electrochemical model and simulates the heat conduction and heat dissipation processes to obtain the cell temperature. The values of the temperature-dependent parameters in the electrochemical model vary with temperature changes.

2.2. Thermal model

Given the significant influence of temperature on the behavior and performance of LIBs, we further integrated a thermal model into the electrochemical model to account for thermal dynamics. This integration incorporates 16 temperature-dependent parameters to capture these effects, following the model proposed by Kumaresan et al. [27]. Beyond the initial cell temperature T_{init}, the cell's heat generation over time also affects its performance. The temperature dependence of the reaction rates k^+ and k^-, the electrolyte diffusion coefficient D_e, electrolyte conductivity σ_e, and the particle diffusion coefficients in the active material $D_{s,p}$ and $D_{s,n}$ are described by the Arrhenius equation as follows,

$$X = X_{ref} \cdot exp(\frac{E_{A,X}}{R}(\frac{1}{T_{ref}} - \frac{1}{T})) \quad (1)$$

where X stands for each of the temperature-dependent parameters [28]. Eq. (1) determines the value of X at temperature T using the corresponding activation energy $E_{A,X}$ and the reference value X_{ref} at the reference temperature T_{ref}, with R being the universal gas constant.

The thermal model used in this work considers three different heat sources: ohmic heat Q_{ohm}, irreversible heat Q_{rxn}, and reversible heat Q_{rev} [29]. These heat source terms, also called heat generation rates, were implemented as follows: The total heat $Q_{tot} = Q_{ohm} + Q_{rxn} + Q_{rev}$, with units of $[\frac{W}{m^3}]$, represents the sum of the individual heat generation rates. All three heat terms are necessary to describe the heat development in the electrodes accurately. The irreversible heat Q_{rxn}

describes the energy required to drive electrochemical reactions and is expressed as follows,

$$Q_{rxn,i} = Fa_i j(x,t)\eta_i(x,t), i \in \{+,-\} \tag{2}$$

where + and − denote the cathode and anode, respectively. The irreversible heat Q_{rxn} is a function of the ionic flux $j(x,t)$ and the overpotential $\eta_i(x,t)$, with F representing the Faraday constant and a_i denoting the ratio of particle surface area to volume.

The reversible generation rate Q_{rev} arises from the entropy changes associated with alterations in the lattice structure of the active material [30] and can be calculated for both cathode and anode as follows,

$$Q_{rev,i} = Fa_i j(x,t)T(x,t)\frac{\partial U_i}{\partial T}\bigg|_{T_{ref}}, i \in \{+,-\} \tag{3}$$

where the temperature is represented by $T(x,t)$, the open circuit voltage (OCV) by U, and the entropic variation of the OCV by $\frac{\partial Ui}{\partial T}$ [26].

The ohmic heat in both electrodes is composed of two main components: electronic transport heat in the solid phase and ion transport heat in the liquid phase, which can be represented as follows,

$$Q_{ohm,i} = \sigma_{eff,i}\left(\frac{\partial \phi_s(x,t)}{\partial x}\right)^2 + \kappa_{eff,i}\left(\frac{\partial \phi_e(x,t)}{\partial x}\right)^2 + \frac{2\{\kappa_{eff,i}RT(x,t)\}}{F}(1-t_+^0) \times \frac{\partial lnc_e(x,t)}{\partial x}\frac{\partial \phi_e(x,t)}{\partial x}, i \in \{+,-\} \tag{4}$$

where the first term represents the electronic transport heat in the solid phase, and the last two represent the ion transport heat in the liquid phase. The coefficient of effective solid-phase conductivity is represented as $\sigma_{eff,i}$, the solid potential is denoted by $\phi_s(x,t)$, the electrolyte potential is indicated by $c_e(x,t)$, while the effective conductivities of the electrolyte is denoted by $\kappa_{eff,i}$. The ohmic heat in the separator $Q_{ohm,s}$ is the only heat source of the separator and can be calculated using Eq. (4) without the first term.

The temperature of the electrodes, taking into account the effects of reversible heat Q_{rev}, can be described as follows,

$$\rho_i C_{p,i}\frac{\partial T_i(x,t)}{\partial t} = \frac{\delta}{\delta x}[\lambda_i \frac{\partial T_i(x,t)}{\partial x}] + Q_{ohm,i} + Q_{rxn,i} + Q_{rev,i}, i \in \{+,-\} \tag{5}$$

where T_i represents the temperature of the electrode, ρ_i represents the volumetric mass density, $C_{p,i}$ denotes the specific heat capacity, λ_i stands for the thermal conductivity, and L_i indicates the thickness of the electrode or separator. The temperature of the separator can be calculated using Eq. (5) whereby $Q_{ohm,s}$ is the only heat source.

The dissipation of heat into the environment is described by the following two equations:

$$-\lambda_a \frac{\partial T_i(x,t)}{\partial x}\bigg|_{x=0} = h_{cell}(T_{amb} - T(x,t)) \tag{6}$$

$$-\lambda_z \frac{\partial T_i(x,t)}{\partial x}\bigg|_{x=L} = h_{cell}(T(x,t) - T_{amb}) \tag{7}$$

These equations account for a constant ambient temperature T_{amb}, which remains unchanged throughout the simulation and corresponds to the initial temperature of the cell. The positive and negative current collectors are denoted with $i \in a,z$, and $T(x,t)$ stands for the temperature of the current collector at a given time. In these equations, the equivalent heat exchange coefficient h_{cell} describes the strength of the heat exchange between the battery and the environment.

3. Parameter benchmarking

For variance-based sensitivity analysis methods, various factors, particularly parameter boundaries, can significantly influence parameter sensitivity. Therefore, establishing accurate value ranges for each parameter based on material properties and battery cell specifications is essential. This ensures that the results of the sensitivity analysis accurately reflect real-world conditions. This work focuses on lithium nickel manganese cobalt oxide (NMC)/graphite cells, which are widely used in the automotive industry due to their high energy density [31]. The experiments were conducted using a Li-ion pouch cell manufactured by KOKAM with a nominal capacity of 7.5 Ah. Post-mortem analysis revealed that the cell structure comprises 23 double-coated anode sheets, along with 22 double-coated and two single-coated cathode sheets. The battery used in this study is shown in Figure S1, and its specifications are summarized in Table S3 of the supplementary materials.

The value ranges for the electrochemical parameters are derived from our previous work [15], which compiled these values from over 20 literature sources along with laboratory experiments and measurements. These parameters have been categorized into four groups, as shown in Table 1, to enable a more detailed assessment of the sensitivity levels of the parameters and their influence on the model's accuracy.

The thermal model parameters are categorized into three groups: material thermal properties, heat dissipation, and activation energies. The first group includes the volumetric mass density ρ^i, the specific heat capacities C_p^i, and the thermal conductivities λ^i, where $i \in \{+, sep, -\}$. The equivalent heat exchange coefficient h_{cell}, which characterizes the heat exchange with the environment, significantly affects the battery temperature. Five activation energy parameters are used to correct the temperature-dependent parameters, i.e., the solid-phase diffusion coefficients, the reaction rate constants, and the liquid-phase conductivity, through the Arrhenius equation described by Eq. (1).

Table 1 summarizes the 39 parameters of the ECTM introduced above, including 23 electrochemical modeling parameters and 16 thermal modeling parameters, with their value ranges and sources. It should be noted that the parameters summarized in this work are only applicable to NMC/graphite cells and not to other cells with different electrode materials. In addition, certain parameters, such as electrolyte conductivity, open circuit potential, and enthalpy change of open circuit potential, are a function of the cell's internal state. The specific settings of these parameters can be found in the supplementary material, while the analysis of the polynomial fitting for these parameters is beyond the scope of this work. Based on the value ranges of the 39 parameters of the ECTM applicable to NMC cells, the sensitivity analysis methodology using the Sobol index (SI) will be introduced in the following sections.

4. Global sensitivity analysis

In this section, the methodology used for the GSA for all 39 parameters of the ECTM, considering both the terminal voltage $V(t)$ and the cell temperature $T(t)$ in the analysis, is described in detail. The terminal voltage can be expressed as the difference between the potentials of the solid phase Φ_s of the electrodes:

$$V(t) = \Phi_s(0^+,t) - \Phi_s(0^-,t) \tag{8}$$

where 0^+ and 0^- correspond to the boundaries between current collectors and electrodes, as shown in Fig. 1. For temperature, we will analyze the parameters' sensitivity using the one-dimensional model's average temperature as the output. This section explains how the first-order, second-order, and total-order Sobol Indices are calculated and what they mean in our setting described above.

4.1. Methodology

For the GSA, the parameters and their boundaries described in the parameter benchmarking in Section 3 are used, with the median values of the determined intervals set as nominal values. The sensitivity of all 39 parameters was analyzed individually by applying Sobol's method to investigate the output variance of the model against the variance of one, two, or all input parameters of the model at the same time, as illustrated in Fig. 2, where the procedure of the GSA is explained.

As shown in Fig. 2, analyzing the effect of operating conditions on parameter sensitivity is one of the highlights of this work. Here,

Table 1
List of ECTM parameter value ranges for the sensitivity analyses.

Physical meaning	Parameter	Unit	Description	Benchmarking	Boundaries
Geometry	L^+	µm	Cathode thickness	74 [32], 36.4 [33], 78 [34], 47 [35], 70 [36], 79 [37], 60 [38], 54.5 [10]	35 – 79
	L^{sep}	µm	Separator thickness	25 [32,33,37,39], 20 [34,35,38], 19 [10], 10-30 [40]	10 – 30
	L^-	µm	Anode thickness	62 [32], 50 [33], 81 [34], 52 [35], 63 [36], 67 [37], 90 [38], 73.7 [10]	35 – 79
	A_{area}	m^2	Electrode surface area	Experimental measurement of Kokam cell	0.378 – 0.395
	ε_s^+	–	Cathode active material volume fraction	0.38 [32], 0.5 [36], 0.375 [37], 0.428 [10]	0.35 – 0.5
	ε_s^-	–	Anode active material volume fraction	0.45 [32], 0.42 [36], 0.419 [37], 0.4 [10]	0.4 – 0.5
	ε_e^+	–	Cathode electrolyte volume fraction	0.45 [32], 0.330 [33], 0.281 [34], 0.27 [35], 0.35 [36], 0.33 [38], 0.296 [10], 0.3 [41]	0.27 – 0.45
	ε_e^{sep}	–	Separator electrolyte volume fraction	0.5 [32], 0.5 [33,37,38], 0.4 [41], 0.46 [34], 0.4 [35], 0.508 [10]	0.4 – 0.55
	ε_e^-	–	Anode electrolyte volume fraction	0.5 [32], 0.332 [33], 0.264 [34], 0.34 [35], 0.33 [36,38], 0.329 [10], 0.3 [41]	0.26 – 0.5
	R_p^+	µm	Cathode particle radius	5 [34,35,39,41], 1.2 [36], 7 [37], 6.49 [10]	1 – 11
	R_p^-	µm	Anode particle radius	10 [34,35], 5 [39,41], 11 [37], 8.7 [10]	1 – 11
Kinetics	κ^+	$\frac{m^{2.5}}{s \cdot mol^{0.5}}$	Cathode reaction rate coefficient	$2 \cdot 10^{-11}$ [32,36,37], $4.38 \cdot 10^{-11}$[35], $3.01 \cdot 10^{-11}$ [10]	$1 \cdot 10^{-11} - 1 \cdot 10^{-10}$
	κ^-	$\frac{m^{2.5}}{s \cdot mol^{0.5}}$	Anode reaction rate coefficient	$2 \cdot 10^{-11}$ [32,37], $1.63 \cdot 10^{-11}$ [35], $1.45 \cdot 10^{-11}$ [10]	$1 \cdot 10^{-11} - 2 \cdot 10^{-10}$
	R_{SEI}	Ωm^2	Anode SEI film resistance	$1 \cdot 10^{-2}$ [34], $3.5 \cdot 10^{-3}$ [37], $1 \cdot 10^{-3}$ [42]	$1 \cdot 10^{-3} - 1 \cdot 10^{-2}$
Lithium concentration	$c_{s,max}^+$	$\frac{mol}{m^3}$	Cathode maximum ionic concentration	51 500 [32], 49 242 [37], 48 580 [10], 49 500 [39,42], 51 830 [41]	48 000 – 52 000
	$c_{s,max}^-$	$\frac{mol}{m^3}$	Anode maximum ionic concentration	31 370 [32], 29 862 [37], 31 920 [10], 30 900 [39], 31 080 [41], 30 555 [42]	29 000 – 33 000
	$c_{e,0}$	$\frac{mol}{m^3}$	Initial electrolyte concentration	1000 [10,35], 1200 [33,34,38,39,41,42]	1000 – 1200
Ion and electron transport	D_s^+	$\frac{m^2}{s}$	Cathode solid diffusion coefficient	$3 \cdot 10^{-14}$ [32,34,35], $3.97 \cdot 10^{-14}$ [38], $2 \cdot 10^{-14}$ [39,41], $8 \cdot 10^{-14}$ [42]	$1 \cdot 10^{-14} - 1 \cdot 10^{-13}$
	D_s^-	$\frac{m^2}{s}$	Anode solid diffusion coefficient	$3 \cdot 10^{-14}$ [32], $1.75 \cdot 10^{-14}$ [34], $2 \cdot 10^{-14}$ [38], $1.54 \cdot 10^{-14}$ [39], $1.4 \cdot 10^{-14}$ [41], $8.8 \cdot 10^{-14}$ [42]	$1 \cdot 10^{-14} - 1 \cdot 10^{-13}$
	D_e	$\frac{m^2}{s}$	Electrolyte diffusion coefficient	$2.6 \cdot 10^{-10}$ [33,38], $2.4 \cdot 10^{-10}$ [10], $1.5 \cdot 10^{-10} - 4.5 \cdot 10^{-10}$ [43], $2 \cdot 10^{-10} - 4.5 \cdot 10^{-10}$ [44]	$1.5 \cdot 10^{-10} - 4.5 \cdot 10^{-10}$
	t_0^+	–	Transference number of lithium cation	0.38 [32,41,42], 0.363 [33,38], 0.26 [10], 0.37-0.43 [43], 0.25 - 0.4 [45], 0.36 - 0.4 [46]	0.25 – 0.43
	σ_s^+	$\frac{S}{m}$	Cathode electrode conductivity	36-185 [47]	36 – 185
	σ_s^-	$\frac{S}{m}$	Anode electrode conductivity	1-10 000 [48]	1 – 10 000
Material thermal properties	C_p^+	$\frac{J}{kg\ K}$	Cathode specific heat capacity	750.5 [49], 849 [50], 1106 [51], 1270 [52], 940 [53], 700 [26], 1260.2 [54]	500–1500
	C_p^{sep}	$\frac{J}{kg\ K}$	Separator specific heat capacity	1718 [49], 2310 [50], 1883 [51], 1978 [52], 1907 [53], 700 [26], 1978 [54]	500–2500
	C_p^-	$\frac{J}{kg\ K}$	Anode specific heat capacity	759.3 [49], 693 [50], 1095 [51], 1437 [52], 940 [53], 700 [26], 1437.4 [54]	500–1700
	λ^+	$\frac{W}{m\ K}$	Cathode thermal conductivity	1.75 [49], 1 [51], 1.58 [52], 2.1 [26], 1.48 [54]	1–3
	λ^{sep}	$\frac{W}{m\ K}$	Separator thermal conductivity	0.22 [49], 0.5 [51], 0.34 [52], 0.16 [26], 0.33 [54]	0.1–1
	λ^-	$\frac{W}{m\ K}$	Anode thermal conductivity	10.88 [49], 1 [51], 1.04 [52], 1.7 [26], 1.04 [54]	1–11
	ρ^+	$\frac{kg}{m^3}$	Cathode volumetric mass density	4476 [49], 4800 [51], 2895 [52], 4670 [53], 2500 [26]	2000–5000
	ρ^{sep}	$\frac{kg}{m^3}$	Separator volumetric mass density	989.6 [49], 900 [51], 1017 [52], 1009 [53], 1100 [26]	800–1200
	ρ^-	$\frac{kg}{m^3}$	Anode volumetric mass density	2310 [49], 2090 [51], 1437 [52], 2260 [53], 2500 [26]	1300–2700
Heat dissipation	h_{cell}	$\frac{Wm^2}{K}$	Equivalent heat exchange coefficient	6.9 [53], 10 [51], 8.7 [55], 6 [28]	1–10

(*continued on next page*)

Table 1 (*continued*).

Activation energy	E_{A,D_s^+}	$\frac{kJ}{mol}$	Activation energy for D_s^+	40 [51], 49.6 [53], 5 [26], 35 [28], 20 [56], 80.6 [10], 25 [41]	5–85
	E_{A,D_s^-}	$\frac{kJ}{mol}$	Activation energy for D_s^-	35 [51], 28.8 [53], 5 [26], 35 [28], 35 [56], 40.8 (30.3) [10], 30 [41]	5–50
	E_{A,D_e}	$\frac{kJ}{mol}$	Activation energy for D_e	17.12 [51], 16.5 [53], 10 [28], 17.1 [10]	10–20
	E_{A,k_p}	$\frac{kJ}{mol}$	Activation energy for k^+	30 [51], 78.1 [53], 5 [26], 20 [28], 30 [56], 43.6 [10], 58 [41]	5–80
	E_{A,k_n}	$\frac{kJ}{mol}$	Activation energy for k^-	53.4 [51], 48.9 [53], 5 [26], 20 [28], 30 [56], 53.4 [10], 32 [41]	5–60
	E_{A,σ_e}	$\frac{kJ}{mol}$	Activation energy for σ_e	4 [53], 20 [28], 17.1 [10]	4–20

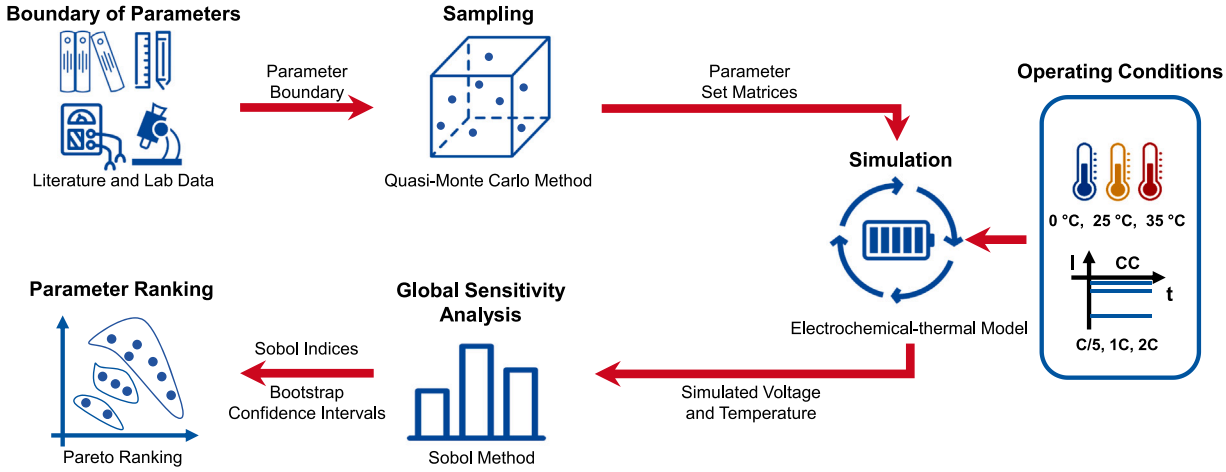

Fig. 2. Framework of the global sensitivity analysis using Sobol method.

we analyzed the impact of ambient temperature and discharge rate on parameter identifiability. The reason is that they directly affect the core physical processes inside the battery, and relevant parameters in the model control these processes, so these parameters exhibit sensitivity to temperature and current rate. Three ambient temperatures, 0 °C, 25 °C, and 35 °C were chosen for the study. The temperature of 0 °C represents a lower bound as it is the minimum allowed charging temperature of the cell. Similarly, 35 °C ambient temperature, and therefore the initial temperature of the battery cell, was chosen so that the maximum allowed charging temperature of the cell is not exceeded. These limits are also the generally accepted window for safe operation [57]. Thus, 25 °C, the median value, was chosen as the reference temperature in Eq. (1) to correct the temperature-dependent parameters. Constant current discharge was analyzed for all temperatures at different current rates of 0.2 C, 1 C, and 2 C.

4.2. Quasi Monte-Carlo method

Unlike traditional Monte Carlo (MC) methods, which rely on random input sequences, the quasi-Monte Carlo (QMC) method utilizes quasi-random, low-discrepancy sequences, ensuring a uniform distribution of input values and thereby avoiding gaps in sampling. This enhances the accuracy and convergence of variance-based GSA. For increasing entries, the uniform distribution of these entries is reduced. The distribution of 100 samples for four variables using the QMC method is illustrated in Fig. 3(a), where the different sizes of the dots indicate the distribution in the fourth dimension. The projections of these samples in three planes in 3D space are shown in Fig. 3(b), demonstrating the good performance of this sampling method for high-dimensional problems. The voltage and temperature profiles of the ECTM simulated at an ambient temperature of 25 °C and 1 C discharging for a given parameter matrix with 500 samples are shown in Fig. 3(c) and (d), respectively. The red dashed curves indicate the simulated voltages and temperatures when all parameters are taken to their mean values for the given boundaries. This approach was chosen to reduce the computational cost compared to the Monte-Carlo method, where more than 10,000 simulations per input parameter would be necessary to generate accurate results with an uncertainty of the estimated SI $\leq$ 10% [18]. We carried out a convergence analysis that showed a number of $n = 2000$ to give robust results for the total-order Sobol index S_{Ti}. The convergent analysis results are shown in Figure S2 in the supplementary materials. In order to obtain first and second-order sensitivity indices with high confidence, we used a sampling number of 10,000 in this work.

4.3. Computation of sensitivity indices

The exclusive influence or so-called main effect of a parameter X_i of the model on the output Y without interaction with other inputs is described by the first-order sensitivity, where the model's total variance normalizes the partial contribution to the variance. Here X_i describes the ith parameter of the model parameters X, $X_{\sim i}$ represents all parameters but X_i. $E_{X_{\sim i}}(Y|X_i)$ is the mean value of the output for all possible input combinations at constant X_i. The first-order sensitivity index S_i of the parameter X_i can be calculated as follows:

$$S_i = \frac{V_i}{V(Y)} = \frac{V_{X_i}(E_{X_{\sim i}}(Y|X_i))}{V(Y)}. \tag{9}$$

Normalizing the variance V_{ij} of the output caused by the inputs X_i and X_j with the total variance of the model $V(Y)$ results in the second-order sensitivity S_{ij}:

$$S_{ij} = \frac{V_{ij}}{V(Y)}. \tag{10}$$

Eq. (10) of the second-order sensitivity indices exclusively represents the additional contribution to the variance in the model output of the interaction effect of the two input parameters X_i and X_j that were varied simultaneously, while their first-order effects are subtracted.

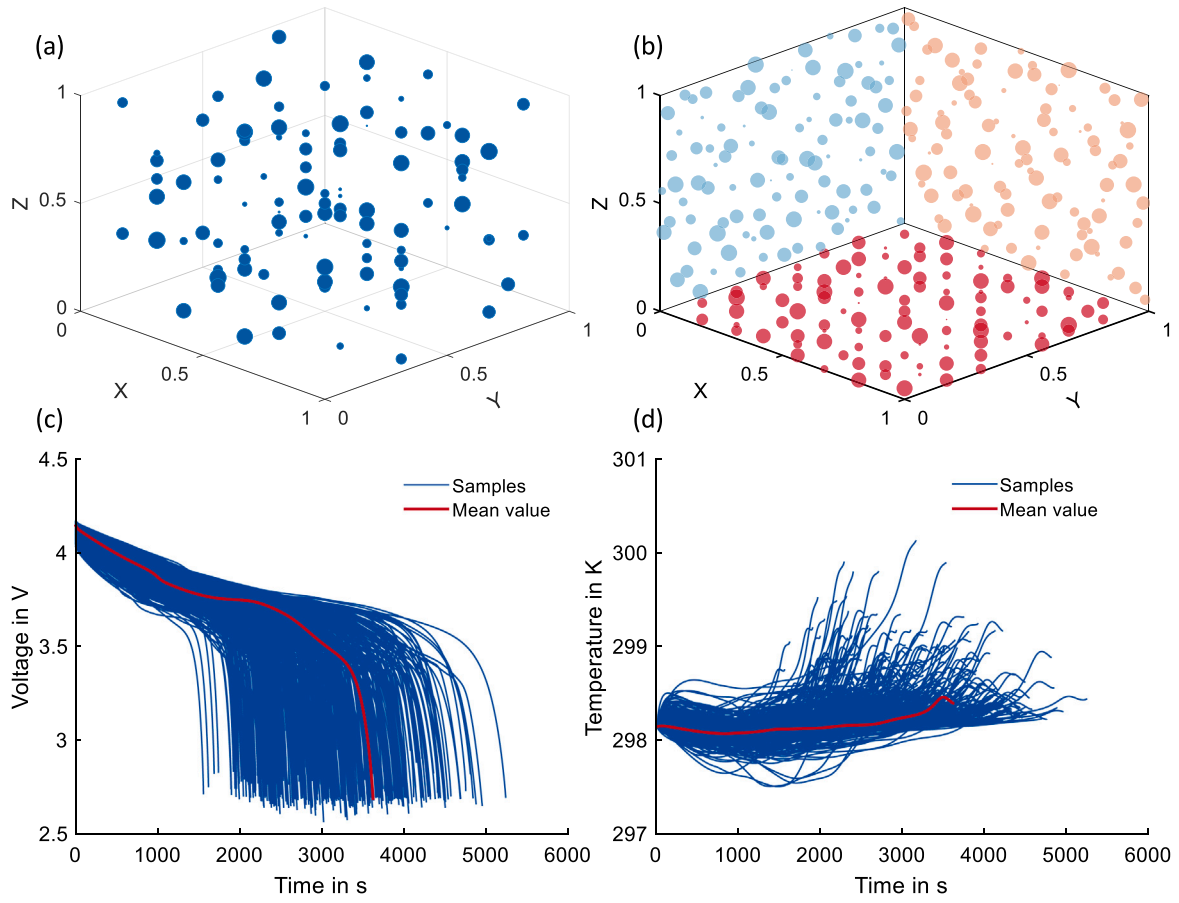

Fig. 3. Sampling using the quasi-Monte Carlo method with 100 samples in four dimensions, with point size denoting the fourth dimension, and simulation results of 500 samples in the given parameter boundary. (a) Sampling in four dimensions and (b) sample projection in three planes. (c) Voltage and (d) temperature simulation results for given parameter sets and the mean value of the value space.

The total-order sensitivity $S_{T_i} = S_i + S_{ij} + \cdots + S_{1\ldots i\ldots k}$ is defined as the sum of the main effect S_i and all higher-order interaction effects that can be attributed to that input parameter and therefore represents the total variance in the terminal voltage or cell temperature due to a change of the value of this parameter X_i:

$$S_{T_i} = \frac{E_{\boldsymbol{X}_{\sim i}}(V_{X_i}(Y|X_{\sim i}))}{V(Y)} = 1 - \frac{V_{\boldsymbol{X}_{\sim i}}(E_{X_i}(Y|\boldsymbol{X}_{\sim i}))}{V(Y)}. \tag{11}$$

In the above formulas for different SIs, the output Y is the root mean square error (RMSE) between the model output and a reference profile that was the simulation result of using the central values of the parameters. For the terminal voltage $V(t)$, the RMSE can be calculated as follows:

$$RMSE = \sqrt{\frac{1}{N_t}\sum_{i=1}^{N_t}(V_i - V_{ref,i})^2} \tag{12}$$

where N_t is the number of data points, V_i is voltage in the ith data point for the given parameter set, and $V_{ref,i}$ is the voltage in the ith data point of the reference profile. The RMSE for the temperature is computed analogously. The specific formulas for calculating the first-order, second-order, and total-order Sobol sensitivity indices are provided in the supplementary materials for reference.

4.4. Bootstrap confidence intervals for the Sobol indices

The results of Sobol index calculations are subject to sampling errors, and to quantify this uncertainty, Bootstrap Confidence Intervals (BCIs) are employed. This method provides a robust way to estimate the variability of the indices, offering more reliable and precise uncertainty quantification. We constructed the 95% and 50% confidence intervals for the first- and total-order Sobol indices S_i and S_{Ti} using the bootstrap method in this work. To compute the BCIs, we resampled the 10,000 model evaluations obtained through QMC, performing 10,000 resamples with replacement, and used the MATLAB bias-corrected percentile method. While resampling a number of 1000 or 2000 is often utilized in practice, a higher count can yield better and more robust estimates for the BCIs, especially for larger percentiles. These numbers also demonstrated promising results compared to the 10,000 resamples reported in this work. However, since the model is not re-evaluated during the re-sampling and the computational cost and time required are low, choosing this higher number is not prohibitive or an issue in practice.

4.5. Pareto ranking of the ECTM parameters

This paper aims to identify the most critical parameters considering multiple outputs, which can be done via a Pareto ranking using the concept of Pareto dominance [58]. The parameters that maximize both the total SIs for terminal voltage and cell temperature simultaneously are more influential and more dominant than other parameters whose indices are smaller. First, we categorize the key parameters as the first group in the Pareto ranking. These key parameters are the ones without any other parameters in the upper right quadrant, which means there is no parameter for which the sensitivity indices for terminal voltage and cell temperature are simultaneously higher than these key parameters. The first group of parameters was then excluded, and the same procedure was used to find the key parameters among the remaining parameters and categorize them into the second group of Pareto ranking. The procedure is repeated until all parameters have been grouped.

5. Results and discussion

This section discusses the global sensitivity analysis results using the Sobol method for the NMC/graphite cell. Firstly, the ECTM parameters were ranked based on their total-order sensitivity magnitudes. Their first- and second-order sensitivity indices were analyzed during a discharge at 1 C and a temperature of 25 °C. Next, we examined the impact of different operating conditions, i.e., ambient temperature and current rate, on the total-order sensitivity of the parameters. Detailed explanations are provided for these effects. Subsequently, we employed the Pareto ranking method to sort the parameters, considering their influence on multiple outputs. By comparing the sensitivity indices of the parameters and analyzing the impact of operating conditions, valuable insights were obtained to optimize the parameter identification process and data selection in the future. The parallel computation was conducted in MATLAB using the High-Performance Computing service from RWTH to expedite the computational process.

5.1. Sobol indices of terminal voltage

In Fig. 4(a), we present the ranking of the 15 most influential parameters based on their total-order SIs of the terminal voltage. The 95% and 50% Bootstrap Confidence Intervals are calculated for both total-order and first-order SIs. In addition, the sensitivity distributions of the two highest-ranked parameters are given in Fig. 4(b), demonstrating that the confidence intervals for total-order SI are smaller than that of first-order SI. Among them, the cathode thickness L^+ has the largest total-order SI, more than 0.7, and first-order SI, about 0.3, as it determines the usable capacity of the cell. Apart from L^+, the sensitivity of the remaining six capacity-related parameters and specific impedance-related parameters are also relatively high, determining the solid-phase diffusion effect and reaction rate. The variation of these parameters affects the impedance properties of the battery and, thus, the time to reach the final cutoff voltage in the discharge, affecting the battery's usable capacity. However, the thermal model parameters have less effect on the terminal voltage than the electrochemical model parameters in this operating condition.

Based on the ranking of the sensitivities, the parameter interactions among the ten most sensitive parameters are revealed in Fig. 4(c). The white squares in the lower triangle on the left side of the graph indicate no interaction or a fragile interaction between the two parameters. The upper triangle is intentionally empty to capture the interactions only once. The most vital interaction occurs between the cathode thicknesses L^+ and anode thickness L^- as the second-order SI between them is more significant than 0.1, because both the cathode and anode determine the capacity of the battery. In addition, there is also a strong interaction between L^+ and the cathode volume fraction of the active material ϵ_s^+, since together they determine the amount of active material available for the cathode. Although the total-order SIs for both cathode and anode thicknesses are high, their first-order indices, which describe the effect of parameter variation alone on the model output, are much lower than the total-order sensitivities. The significant difference between these two illustrates that these parameters strongly interact with other parameters and, therefore, jointly influence the model's output.

5.2. Total-order SI of terminal voltage under different operating conditions

The total-order SI of terminal voltage for 23 electrochemical-model parameters based on the ECTM used in this work under different ambient temperatures and C-rates are shown in Fig. 5, where both the color and size of the markers in the scatter plot indicate the magnitude of the sensitivity. For certain parameters, such as D_s^+, the sensitivity in the highest case is two orders of magnitude greater than in the lowest case, indicating the high impact of test conditions on the parameter identifiability.

As illustrated in the first sub-diagram, the seven capacity-related parameters, i.e., electrode thickness $L^\pm$, volume fraction of active material $\epsilon_s^\pm$, maximum ion concentration $c_{s,max}^\pm$, and electrode surface area A_{area}, show high or medium sensitivity under the given parameter boundaries. The variation of these parameters leads to changes in battery capacity and the OCV curve of the full cell, which further results in significant variations in the terminal voltage under a given load profile. The sensitivity of these parameters is simultaneously related to the ambient temperature and the magnitude of the discharge current. Low temperature affects the charge/discharge characteristics of the LIB by inhibiting the reaction rate, electron transport, and solid- and liquid-phase diffusion, increasing the cell's impedance, which causes the battery to reach the cutoff voltage early, before it is fully discharged or charged, thus resulting in a decline in the battery's capacity. Similarly, LIB also experiences capacity failure as the current rate increases due to severe polarization. Therefore, when the battery is charged or discharged at a low temperature and high current rate, the impact of impedance-related parameters on the model terminal voltage increases, thus exhibiting greater sensitivity. In contrast, the effect of the capacity-related parameters on the terminal voltage is weakened and, thus, their sensitivity is reduced. The cathode and anode solid-phase diffusion coefficient $D_s^\pm$ and particle radius $R_p^\pm$, which determine the performance of lithium-ion diffusion in the electrode active material, show higher sensitivity with decreasing temperatures and increasing C-rate. In addition, the sensitivity of the reaction rate constant $k^\pm$ and the SEI resistance R_{SEI} show the same trend. It should be noted that some impedance-related parameters have the same very low sensitivities under different operating conditions, which may be related to the small boundaries of these parameters. However, this does not mean that the operating conditions do not influence their sensitivities. In particular, varying the value of specific capacity-related parameters can also influence the impedance of LIB. For example, increasing the thickness of the electrode will lead to a more considerable diffusion distance of lithium ions and will increase the concentration difference polarization.

As described in Section 3, we divided the 16 thermal parameters into material thermal property parameters, heat dissipation parameters, and activation energy parameters. The first two categories affect the LIB model's temperature change during operation, indirectly affecting the model's voltage output. The Arrhenius equations apply the activation energy parameters to correct temperature-dependent parameters that affect the impedance properties of the cell due to temperature variation. In Fig. 5, we can also see how the thermal model parameter affects the terminal voltage under different operating conditions. It can be seen that the model is more sensitive to specific activation energy parameters, while the sensitivity of other thermal parameters is very low. Furthermore, comparing the sensitivity of the activation energy with the sensitivity of the corresponding parameter corrected in Fig. 5, it can be observed that they are positively relevant. For example, the solid-phase diffusion coefficients $D_s^\pm$ and the reaction rate constants $k^\pm$ exhibit a considerable sensitivity as well as their corresponding activation energies $E_{A,D_s^\pm}$ and $E_{A,k^\pm}$, while the sensitivity of both the liquid-phase diffusion coefficient D_e and its activation energy E_{A,D_e} are small. Similar to the electrochemical model parameters, the sensitivity of the activation energy parameters is also affected by the ambient temperature and the C-rates. However, their sensitivity does not vary monotonically with ambient temperature. The activation energy parameters have minimal sensitivity when the ambient temperature is 25 °C, due to the slight temperature difference $\frac{1}{T_{ref}} - \frac{1}{T(x,t)}$ at this time. As the current rate increases, the sensitivity of the activation energy parameter also increases, similar to the impedance-related parameters.

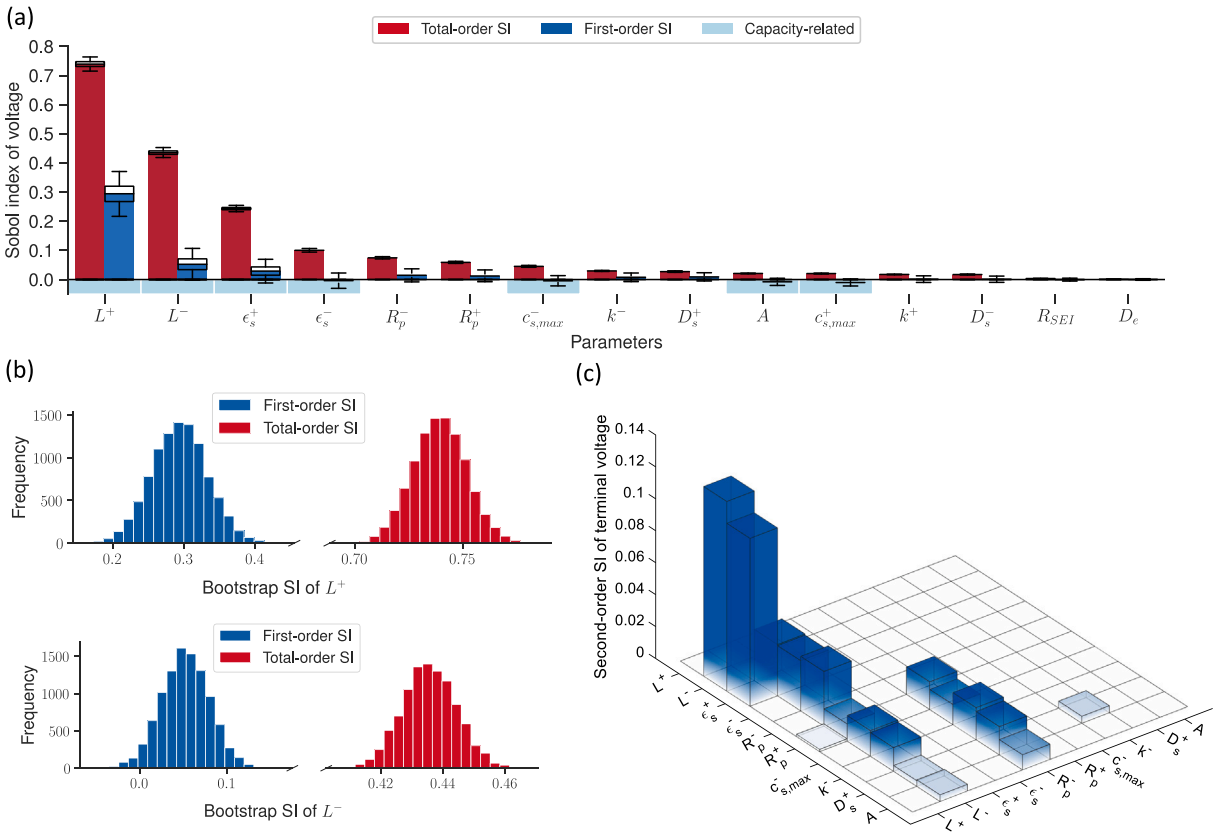

Fig. 4. Sobol indices of the terminal voltage at 25 °C and 1 C discharge. (a) Ranking of the first- and total-order SIs of the terminal voltage for the 15 most sensitive parameters. The parameters in the blue area are related to the capacity. (b) Distribution of the bootstrap sensitivity indices given for the two most important parameters. (c) Second-order SIs. (For interpretation of the references to colour in this figure legend, the reader is referred to the web version of this article.)

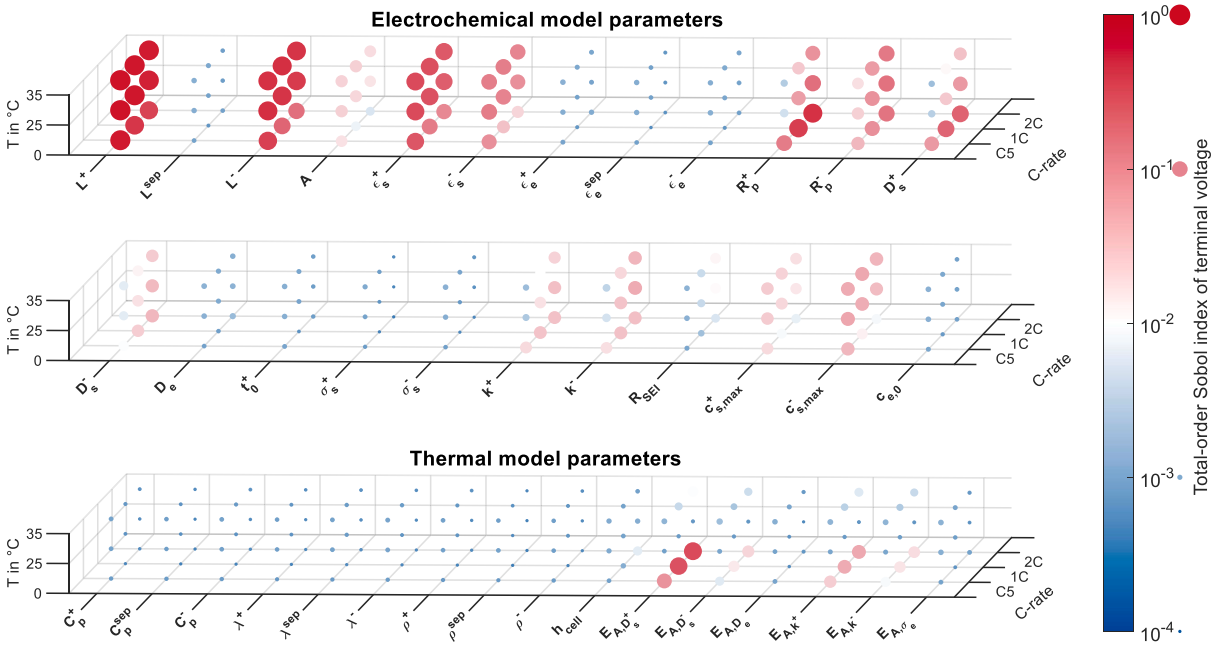

Fig. 5. Total-order SIs of the terminal voltage for all 39 ECTM parameters under different ambient temperatures and C-rates. The color and size of the marker indicate the magnitude of SI. (For interpretation of the references to colour in this figure legend, the reader is referred to the web version of this article.)

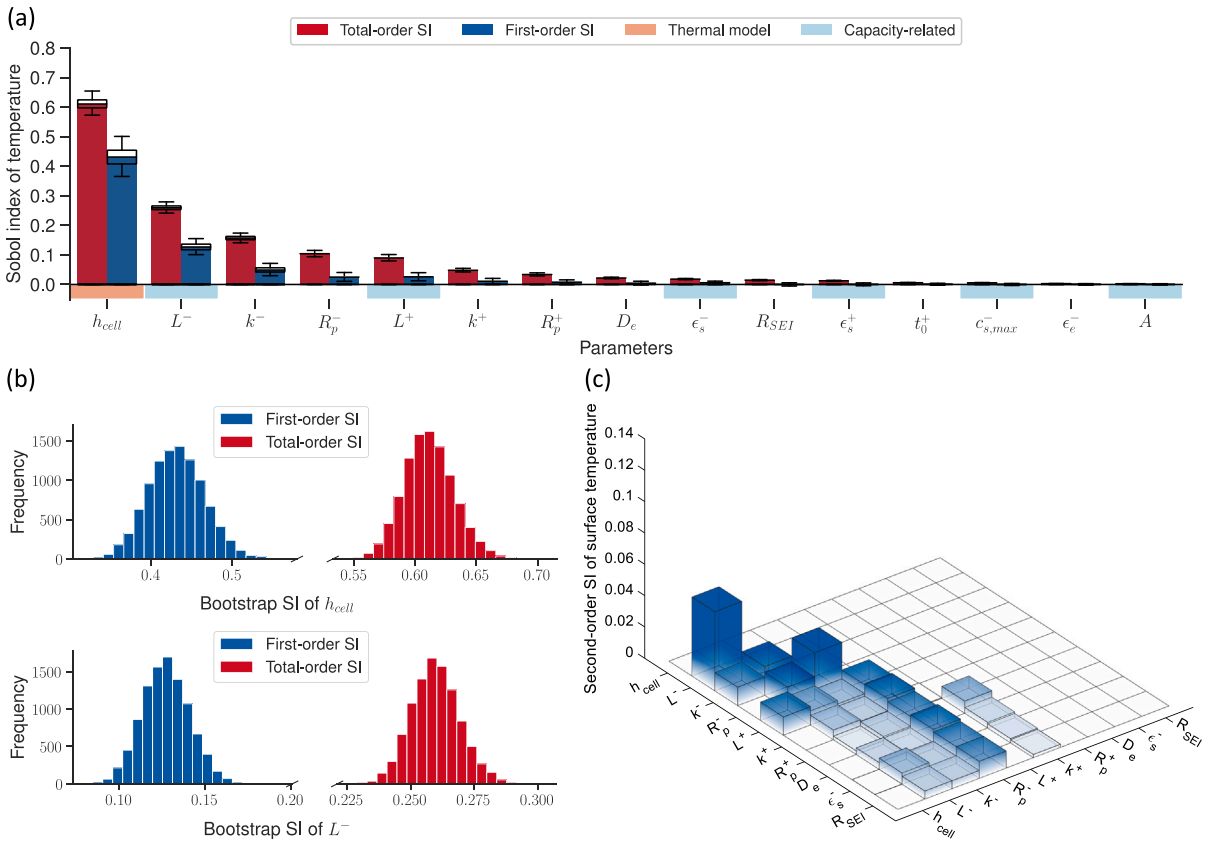

Fig. 6. Sobol indices of the cell temperature at 25 °C and 1 C discharge. (a) Ranking of the first- and total-order SIs of the cell temperature for the 15 most sensitive parameters. The parameters in the blue area and yellow are related to the capacity and thermal model, respectively. (b) Distribution of the bootstrap sensitivity indices given for the two most important parameters. (c) Second-order SIs. (For interpretation of the references to colour in this figure legend, the reader is referred to the web version of this article.)

5.3. Sobol indices of cell temperature

Fig. 6(a) shows the sensitivity of cell temperature to the parameters of the ECTM, and the sensitivity distributions of the two most sensitive parameters are given by Fig. 6(b). The battery temperature is mainly determined by the equivalent heat exchange coefficient h_{cell}, which has a total-order sensitivity index close to 0.5 in this case. However, the cell temperature is not sensitive to the material's thermal properties and the activation energy parameters, whose SI is less than 0.01. The lower sensitivity of the former indicates that the main factor of temperature variation is not the thermal properties but the terms of heat generation and dissipation. The lower sensitivity of the latter is that the ambient temperature is close to the reference temperature in the Arrhenius equations, and the extremely small temperature difference weakens its ability to correct temperature-dependent parameters. In addition, the sensitivity of the capacity-related parameters decreases while the sensitivity of the parameters related to the heat generation rate increases.

The interaction between the ECTM parameters regarding the cell temperature is not as strong as that of the terminal voltage. The maximum second-order sensitivity is less than 0.05, see Fig. 6(c). A relatively strong interaction between the equivalent heat exchange coefficient and the anode thickness is noted. These two parameters have the highest sensitivity with the sum of their first-order sensitivities exceeding 0.5, as shown in Fig. 6(a). The temperature change can be analyzed in three aspects: heat sources, heat dissipation, and thermal properties. The third term is determined by the thermal physical properties, i.e., thermal conductivity and specific heat capacity, and the size of the cell, i.e., thickness. Anode thickness L^- affects the capacity of the cell and thus the heat production on the one hand and determines the size of the negative electrode and hence its ability to store thermal energy on the other hand. Based on the boundary of thermal property parameters given in Table 1, the negative electrode is more likely to have a more remarkable ability to store heat. This also explains the higher sensitivity of the cathode parameters considering voltage output in Fig. 4 compared to the anode, and the higher sensitivity of the anode parameters considering the temperature output in Fig. 6.

5.4. Total-order SI of cell temperature under different operation conditions

Compared to the total-order SIs of terminal voltage, the sensitivity of the ECTM parameters is significantly different when considering the temperature output of the ECTM, as shown in Fig. 7. It is noticeable in Fig. 7 that the sensitivity of all the capacity-related parameters has decreased. However, they still determine the utilization capacity and thus affect the charge/discharge time of the battery, i.e., the length of the voltage and temperature curves. Specific impedance-related parameters, such as the electrolyte volume fraction $\epsilon_e^{\pm}$ and electrolyte diffusion coefficient D_e, hardly affect the terminal voltage but affect the cell temperature. The electrolyte volume fraction is used to correct the effective liquid-phase conductivity $\kappa_{eff}^{\pm}$ together with the Bruggeman coefficient, which plays an essential role in the ohmic heat generation rate, as shown in Eq. (4). The liquid-phase conductivity, which is related to the ohmic heat generation term, is critical to the model temperature output. In addition to the liquid-phase conductivity, the diffusion characteristics of ions in the electrolyte are another key factor affecting the temperature output because it affects the ohmic heat generation rate by changing the lithium ions concentration in the electrolyte, which explains the greater sensitivity of the model's temperature output to the electrolyte volume fraction $\epsilon_e^{\pm}$ and diffusion coefficient D_e. The other two heat source terms, i.e., the heat of reaction Q_{rxn} and reversible heat Q_{rev}, as represented by Eqs. (2) and

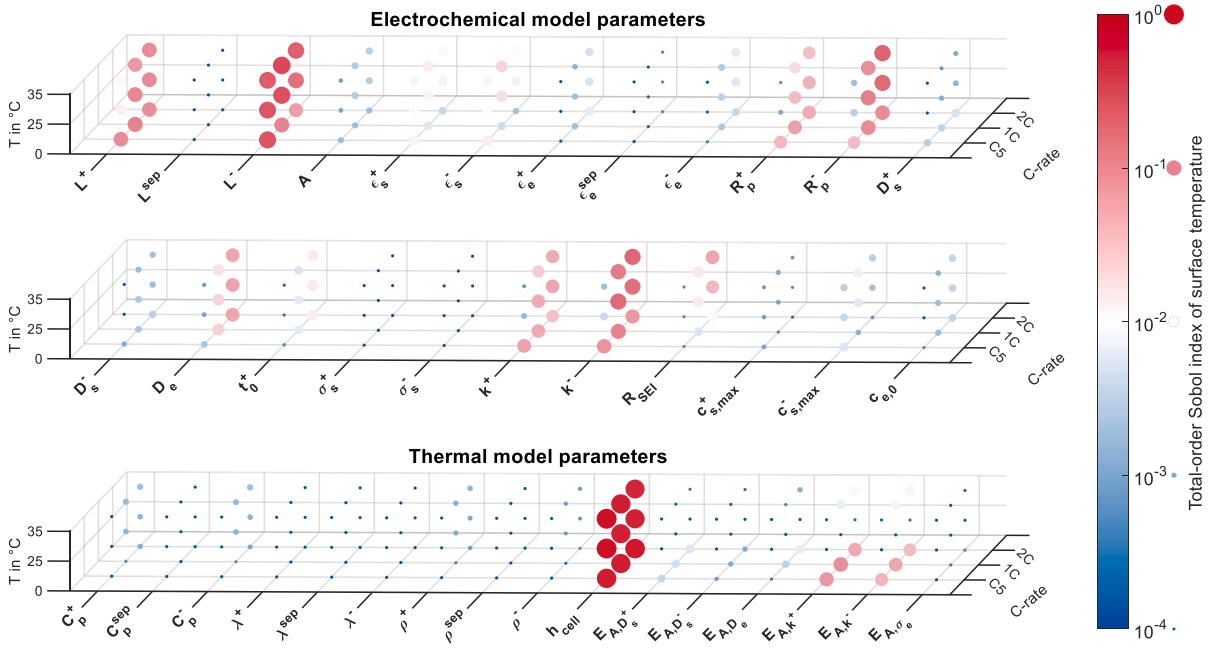

Fig. 7. Total-order Sobol index of the cell temperature for all 39 ECTM parameters under different ambient temperatures and C-rates. The color and size of the marker indicate the magnitude of SI. (For interpretation of the references to colour in this figure legend, the reader is referred to the web version of this article.)

(3), are both influenced by the ionic flow. Therefore, the reaction rate constants remain highly sensitive because the magnitude of the ion flux is directly related to these parameters. However, the importance of the solid-phase diffusion diminishes considering the model temperature output, which is reflected in the sensitivity of the solid-phase diffusion coefficient.

Similar to the voltage output, the ability of the parameters to affect the temperature output is also related to the ambient temperature and C-rates. As the current rate increases, the sensitivity of temperature for most impedance-related parameters increases, as shown in Fig. 7. Under a high current rate, the battery's heat generation power is significant due to the large current exchange density and severe polarization, which leads to a rapid increase in battery temperature. At this time, changes in the magnitude of the impedance-related parameters have a greater impact on the temperature rise curve, thus exhibiting a greater sensitivity. However, the sensitivities of the capacity-related parameters did not show the same variation trend. For example, when the ambient temperature is 0 °C, the negative electrode thickness has the maximum sensitivity under discharging with 0.2 C, while the highest sensitivity was found at 25 °C and 35 °C at under 1 C discharging.

For the thermal model parameters, those indicating the material's thermal properties, including specific heat capacity, volumetric mass density, and thermal conductivity, always show very low sensitivity compared to those related to the heat generation term and the heat dissipation term. This indicates that the temperature output of the model is mainly influenced by the heat generation term as well as the heat dissipation term, rather than the thermal properties. It is obvious that the equivalent heat exchange coefficient h_{cell}, whose total-order sensitivity is greater than 0.4 for all operating conditions, plays an important role in the battery temperature. The reason is that it is the only parameter that describes the heat transfer process between the cell and the environment, which determines the ability of the cell to dissipate heat to the environment. Its sensitivity is affected by the temperature and the current rate, and it is negatively correlated with the sensitivity of the parameters related to the heat generation terms. The sensitivity of the h_{cell} reaches a maximum at 35 °C and 0.2 C discharge because the high temperature and low current rate improve the cell polarization, reduce the heat generation rate, and decrease the sensitivity of the impedance parameters, thus increasing the sensitivity of h_{cell}. Among the six activation energy parameters, only the activation energy parameter used to correct the reaction rate showed sensitivity under low temperatures. Their sensitivity increases as the temperature deviates more from the reference temperature.

5.5. Pareto ranking of the ECTM parameters

To use multi-type data to improve the identification parameters of the ECTM, we must consider the parameters' effect on the model's multiple outputs. Here, we used Pareto ranking, introduced in Section 4.5, to rank all model parameters according to their total-order indices. An example of ranking is illustrated in Fig. 8(a), where 10 parameters are divided into four groups. The Pareto ranking for 25 °C and 1 C current rate is shown in Fig. 8(b) in double logarithmic coordinates, where all parameters are divided into five groups, and the higher ranking of the parameters indicates that the parameters have a greater influence on the voltage output and temperature output of the model, which can provide guidance when determining the values of the parameters using a stepwise identification approach.

The effects of ambient temperature and current rate on the Pareto ranking of the ECTM parameters are summarized in Fig. 8(c), where the marker's color indicates the parameter's Pareto ranking. It can be seen that parameters such as electrode thickness and heat transfer coefficient are of high order at different ambient temperatures and current levels. So, these parameters need to be prioritized and accurately determined during the identification process to avoid the impact on the accurate identification of other parameters. Other parameters related to battery capacity and impedance-related parameters with relatively high sensitivity are ranked as being more influenced by ambient temperature and current magnitude. Therefore, selecting appropriate measurement data can improve the identification results of these parameters. Measured data at higher temperatures and lower currents are suitable for identifying capacity-related parameters, while low temperatures and high currents can increase the ranking of impedance-related parameters. Meanwhile, the ranking of parameters not shown in the figure is always at a lower level for different operating conditions. For parameters that do not significantly affect the output, improving their sensitivity is challenging, even with changes in operating conditions, making it hard to accurately identify their values. These parameter values can

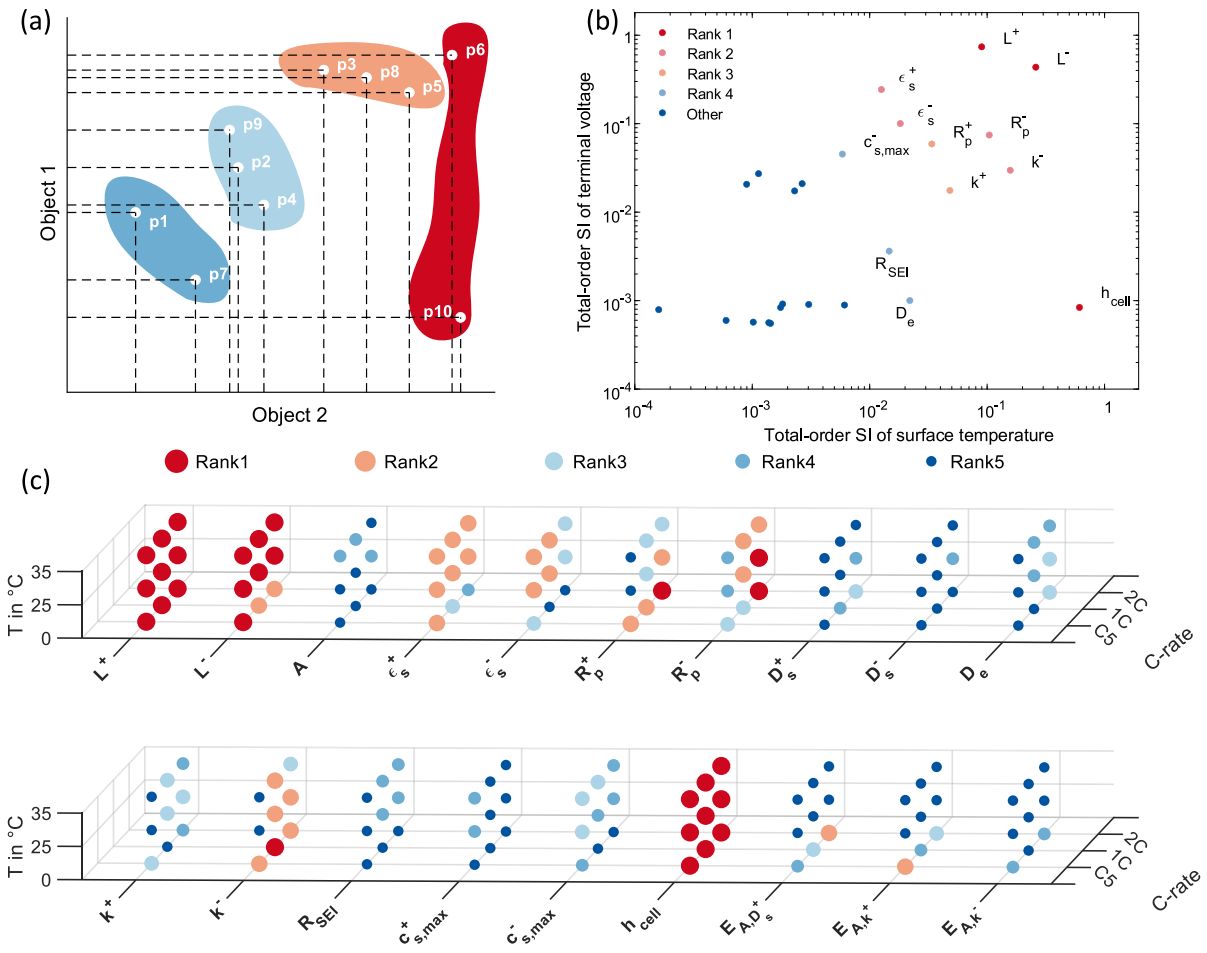

Fig. 8. Pareto ranking result. (a) Schematic diagram of the Pareto ranking method. (b) Grouping of parameter sensitivities under 1 C discharge at 25 °C. (c) Parameter Pareto rank at different temperatures and C-rates. Parameters that do not appear indicate that they are always Rank 5. (For interpretation of the references to colour in this figure legend, the reader is referred to the web version of this article.)

be established by reviewing the literature to evaluate their reference values, which should remain constant throughout the identification process.

5.6. Future work and application

In the future, we aim to explore the possibility of developing a non-invasive method for parameterizing ECTMs with the help of the identifiability analysis framework developed in this work. Fast parameterization of the model by using measured voltage and temperature data greatly reduces time and money costs compared to complex experimental measurement methods, which makes significant sense for the rapid model development of a new generation of batteries. A major research direction is the design of experiments, i.e., how to design suitable working conditions that maximize the information in the obtained measured voltage and temperature data, thus contributing to accurate parameterization. This work focuses on the effects of ambient temperature and discharge current rate on sensitivity, but future work could incorporate additional operating factors such as relaxation segments, dynamic working conditions, and depth of discharge.

This adaptable method can be tailored for use in different battery sub-models. In addition to temperature and voltage outputs, the method can give the effect of parameters on the electrochemical impedance spectra and the aging simulation, which is critical for understanding, developing battery models, and determining key parameters. For the aging models integrated into the electrochemical model, the capacity and power fade of the battery will have different trajectories when different degradation mechanisms and the values of the aging model parameters are chosen. Therefore, analyzing the effects of parameters on the aging behavior of batteries is of great help in constructing aging models applied in different situations.

6. Conclusions

In this paper, a framework for parameter identifiability analysis was developed for the electrochemical thermal coupling model using different types of measurement data, such as terminal voltage and cell temperature, to facilitate non-invasive parameterization. The parameters were rigorously benchmarked through thorough literature reviews and experiments to ensure the reliability of the analysis results. Based on this, the Sobol sensitivity indices were calculated to quantify parameter influence on model outputs and their interactions, considering both voltage and temperature. The proposed framework was implemented on an nickel manganese cobalt oxide/graphite battery, and the impact of operating conditions on parameter identifiability was further analyzed by varying the discharge current rate and ambient temperature. The developed framework can be easily extended and applied to different battery chemistries and can also accommodate a wider range of battery data types. Our analysis has led to some important conclusions:

- Choosing the appropriate test temperature and current rate can increase the sensitivity of certain parameters by up to two orders of magnitude.

- Lowering the test temperature and increasing the current rate can increase the identifiability of impedance-related parameters and reduce the identifiability of capacity-related parameters.
- Excessive heat dissipation minimizes temperature changes, reducing the identifiability of thermal parameters, which must be considered in experimental design.
- To identify the activation energy parameter, tests in a wide temperature range need to be performed.
- Temperature data can help identify specific parameters that have little effect on voltage but are more sensitive to cell temperature.

The findings offer valuable guidance for designing test conditions that facilitate the acquisition of high-quality data for non-invasive parameter identification. In addition, the Pareto ranking method was applied in this work to group parameters when different types of data are considered. In general, the results of the parameter identifiability analysis in this work lay the foundation for developing a non-invasive parameterization framework of an electrochemical thermal coupling model using the easy-to-measure electrical and temperature data.

CRediT authorship contribution statement

Jue Chen: Writing – original draft, Visualization, Validation, Software, Resources, Methodology, Investigation, Conceptualization. **Sven Patrick Mattus:** Writing – review & editing, Methodology, Investigation. **Wenjiong Cao:** Writing – review & editing, Validation, Methodology. **Dirk Uwe Sauer:** Writing – review & editing, Methodology. **Weihan Li:** Writing – review & editing, Supervision, Methodology, Funding acquisition, Conceptualization.

Declaration of competing interest

The authors declare that they have no known competing financial interests or personal relationships that could have appeared to influence the work reported in this paper.

Acknowledgments

This work is supported by the research project “SPEED” (03XP0585), funded by the German Federal Ministry of Education and Research (BMBF), and the research project “ADMirABLE” (03ETE053E), funded by the German Federal Ministry for Economic Affairs and Climate Action (BMWK).

Appendix A. Supplementary data

Supplementary material related to this article can be found online at https://doi.org/10.1016/j.adapen.2025.100221.

Data availability

Data will be made available on request.

References

[1] Cano ZP, Banham D, Ye S, Hintennach A, Lu J, Fowler M, Chen Z. Batteries and fuel cells for emerging electric vehicle markets. Nat Energy 2018;3(4):279–89.
[2] Zhang X, Li Z, Luo L, Fan Y, Du Z. A review on thermal management of lithium-ion batteries for electric vehicles. Energy 2022;238:121652.
[3] Wang Q, Ping P, Zhao X, Chu G, Sun J, Chen C. Thermal runaway caused fire and explosion of lithium ion battery. J Power Sources 2012;208:210–24.
[4] Liu J, Yadav S, Salman M, Chavan S, Kim SC. Review of thermal coupled battery models and parameter identification for lithium-ion battery heat generation in EV battery thermal management system. Int J Heat Mass Transfer 2024;218:124748.
[5] Hu X, Li S, Peng H. A comparative study of equivalent circuit models for Li-ion batteries. J Power Sources 2012;198:359–67.
[6] Wang S, Dang Q, Gao Z, Li B, Fernandez C, Blaabjerg F. An innovative square root-untraced Kalman filtering strategy with full-parameter online identification for state of power evaluation of lithium-ion batteries. J Energy Storage 2024;104:114555.
[7] Wang S, Zhang S, Wen S, Fernandez C. An accurate state-of-charge estimation of lithium-ion batteries based on improved particle swarm optimization-adaptive square root cubature Kalman filter. J Power Sources 2024;624:235594.
[8] Vashisht S, Rakshit D, Panchal S, Fowler M, Fraser R. Experimental estimation of heat generating parameters for battery module using inverse prediction method. Int Commun Heat Mass Transfer 2025;162:108539.
[9] Chaturvedi NA, Klein R, Christensen J, Ahmed J, Kojic A. Algorithms for advanced battery-management systems. IEEE Control Syst Mag 2010;30(3):49–68.
[10] Ecker M, Tran TKD, Dechent P, Käbitz S, Warnecke A, Sauer DU. Parameterization of a physico-chemical model of a lithium-ion battery: I. Determination of parameters. J Electrochem Soc 2015;162(9):A1836.
[11] Schmalstieg J, Sauer DU. Full cell parameterization of a high-power lithium-ion battery for a physico-chemical model: Part II. Thermal parameters and validation. J Electrochem Soc 2018;165(16):A3811.
[12] Li W, Demir I, Cao D, Jöst D, Ringbeck F, Junker M, et al. Data-driven systematic parameter identification of an electrochemical model for lithium-ion batteries with artificial intelligence. Energy Storage Mater 2022;44:557–70.
[13] Park S, Kato D, Gima Z, Klein R, Moura S. Optimal experimental design for parameterization of an electrochemical lithium-ion battery model. J Electrochem Soc 2018;165(7):A1309.
[14] Edouard C, Petit M, Forgez C, Bernard J, Revel R. Parameter sensitivity analysis of a simplified electrochemical and thermal model for Li-ion batteries aging. J Power Sources 2016;325:482–94.
[15] Li W, Cao D, Jöst D, Ringbeck F, Kuipers M, Frie F, et al. Parameter sensitivity analysis of electrochemical model-based battery management systems for lithium-ion batteries. Appl Energy 2020;269:115104.
[16] Song M, Choe S-Y. Parameter sensitivity analysis of a reduced-order electrochemical-thermal model for heat generation rate of lithium-ion batteries. Appl Energy 2022;305:117920.
[17] Saltelli A, Annoni P, Azzini I, Campolongo F, Ratto M, Tarantola S. Variance based sensitivity analysis of model output. Design and estimator for the total sensitivity index. Comput Phys Comm 2010;181(2):259–70.
[18] Iooss B, Lemaître P. A review on global sensitivity analysis methods, uncertainty management in simulation–optimization of complex systems: Algorithms and applications. 2015, p. 101–22.
[19] Appiah WA, Busk J, Vegge T, Bhowmik A. Sensitivity analysis methodology for battery degradation models. Electrochim Acta 2023;439:141430.
[20] van Janse Rensburg A, van Schoor G, van Vuuren PA. Stepwise global sensitivity analysis of a physics-based battery model using the morris method and Monte Carlo experiments. J Energy Storage 2019;25:100875.
[21] Deng Z, Hu X, Lin X, Kim Y, Li J. Sensitivity analysis and joint estimation of parameters and states for all-solid-state batteries. IEEE Trans Transp Electrification 2021;7(3):1314–23.
[22] Borgonovo E, Plischke E. Sensitivity analysis: A review of recent advances. European J Oper Res 2016;248(3):869–87.
[23] Lin N, Xie X, Schenkendorf R, Krewer U. Efficient global sensitivity analysis of 3D multiphysics model for Li-ion batteries. J Electrochem Soc 2018;165(7):A1169.
[24] Streb M, Ohrelius M, Klett M, Lindbergh G. Improving Li-ion battery parameter estimation by global optimal experiment design. J Energy Storage 2022;56:105948.
[25] Wei J, Chen C, Dong G. Global sensitivity analysis for impedance spectrum identification of lithium-ion batteries using time-domain response. IEEE Trans Ind Electron 2022;70(4):3825–35.
[26] Torchio M, Magni L, Gopaluni RB, Braatz RD, Raimondo DM. LIONSIMBA: A matlab framework based on a finite volume model suitable for Li-ion battery design, simulation, and control. J Electrochem Soc 2016;163(7):A1192–205.
[27] Kumaresan K, Sikha G, White RE. Thermal model for a Li-ion cell. J Electrochem Soc 2007;155(2):A164.
[28] Hosseinzadeh E, Genieser R, Worwood D, Barai A, Marco J, Jennings P. A systematic approach for electrochemical-thermal modelling of a large format lithium-ion battery for electric vehicle application. J Power Sources 2018;382:77–94.
[29] Northrop PWC, Ramadesigan V, De S, Subramanian VR. Coordinate transformation, orthogonal collocation, model reformulation and simulation of electrochemical-thermal behavior of lithium-ion battery stacks. J Electrochem Soc 2011;158(12):A1461.
[30] Keyser M, Pesaran A, Li Q, Santhanagopalan S, Smith K, Wood E, et al. Enabling fast charging–battery thermal considerations. J Power Sources 2017;367:228–36.
[31] Salgado R, Danzi F, Oliveira J, El-Azab A, Camanho P, Braga M. The latest trends in electric vehicles batteries. Molecules 2021;26:3188.
[32] Erhard SV, Osswald PJ, Keil P, Höffner E, Haug M, Noel A, et al. Simulation and measurement of the current density distribution in lithium-ion batteries by a multi-tab cell approach. J Electrochem Soc 2017;164(1):A6324–33.
[33] Smith K, Wang C-Y. Solid-state diffusion limitations on pulse operation of a lithium ion cell for hybrid electric vehicles. J Power Sources 2006;161(1):628–39.
[34] Ji Y, Zhang Y, Wang C-Y. Li-ion cell operation at low temperatures. J Electrochem Soc 2013;160(4):A636–49.

[35] Smekens J, Paulsen J, Yang W, Omar N, Deconinck J, Hubin A, et al. A modified multiphysics model for lithium-ion batteries with a LixNi1/3Mn1/3Co1/3O2 electrode. Electrochim Acta 2015;174:615–24.
[36] Stewart SG, Srinivasan V, Newman J. Modeling the performance of lithium-ion batteries and capacitors during hybrid-electric-vehicle operation. J Electrochem Soc 2008;155(9):A664.
[37] Rheinfeld A, Sturm J, Noel A, Wilhelm J, Kriston A, Pfrang A, et al. Quasi-isothermal external short circuit tests applied to lithium-ion cells: Part II. Model Simul J Electrochem Soc 2019;166(2):A151–77.
[38] Nileshwar PR, McGordon A, Ashwin TR, Greenwood D. Parametric optimization study of a lithium-ion cell. Energy Procedia 2017;138:829–34.
[39] Fang W, Kwon OJ, Wang C-Y. Electrochemical-thermal modeling of automotive Li-ion batteries and experimental validation using a three-electrode cell. Int J Energy Res 2010;34(2):107–15.
[40] Lee H, Yanilmaz M, Toprakci O, Fu K, Zhang X. A review of recent developments in membrane separators for rechargeable lithium-ion batteries. Energy Env Sci 2014;7(12):3857–86.
[41] Tanim TR, Rahn CD, Wang C-Y. A temperature dependent, single particle, lithium ion cell model including electrolyte diffusion. J Dyn Syst Meas Control 2015;137(1):0022–434.
[42] Awarke A, Pischinger S, Ogrzewalla J. Pseudo 3D modeling and analysis of the SEI growth distribution in large format Li-ion polymer pouch cells. J Electrochem Soc 2013;160(1):A172–81.
[43] Capiglia C, Saito Y, Kageyama H, Mustarelli P, Iwamoto T, Tabuchi T, et al. 7Li and 19f diffusion coefficients and thermal properties of non-aqueous electrolyte solutions for rechargeable lithium batteries. J Power Sources 1999;81–82:859–62.
[44] Ehrl A, Landesfeind J, Wall WA, Gasteiger HA. Determination of transport parameters in liquid binary lithium ion battery electrolytes. J Electrochem Soc 2017;164(4):A826–36.
[45] Nyman A, Behm M, Lindbergh G. Electrochemical characterisation and modelling of the mass transport phenomena in LiPF6–EC–EMC electrolyte. Electrochim Acta 2008;53(22):6356–65.
[46] Valoen LO, Reimers JN. Transport properties of LiPF[sub 6]-based Li-ion battery electrolytes. J Electrochem Soc 2005;152(5):A882.
[47] Chen Y-H, Wang C-W, Zhang X, Sastry AM. Porous cathode optimization for lithium cells: Ionic and electronic conductivity, capacity, and selection of materials. J Power Sources 2010;195(9):2851–62.
[48] Park M, Zhang X, Chung M, Less GB, Sastry AM. A review of conduction phenomena in Li-ion batteries. J Power Sources 2010;195(24):7904–29.
[49] Werner D, Loges A, Becker DJ, Wetzel T. Thermal conductivity of Li-ion batteries and their electrode configurations – a novel combination of modelling and experimental approach. J Power Sources 2017;364:72–83.
[50] Maleki H, Wang H, Porter W, Hallmark J. Li-ion polymer cells thermal property changes as a function of cycle-life. J Power Sources 2014;263:223–30.
[51] Lin N, Xie X, Schenkendorf R, Krewer U. Efficient global sensitivity analysis of 3D multiphysics model for Li-ion batteries. J Electrochem Soc 2018;165(7):A1169–83.
[52] Mei W, Chen H, Sun J, Wang Q. The effect of electrode design parameters on battery performance and optimization of electrode thickness based on the electrochemical–thermal coupling model. Sustain Energy & Fuels 2019;3(1):148–65.
[53] Liebig, Gupta, Kirstein, Schuldt, Agert. Parameterization and validation of an electrochemical thermal model of a lithium-ion battery. Batteries 2019;5(3):62.
[54] Sheng L, Su L, Zhang H. Experimental determination on thermal parameters of prismatic lithium ion battery cells. Int J Heat Mass Transfer 2019;139:231–9.
[55] Tippmann S, Walper D, Balboa L, Spier B, Bessler WG. Low-temperature charging of lithium-ion cells part I: Electrochemical modeling and experimental investigation of degradation behavior. J Power Sources 2014;252:305–16.
[56] Lyu P, Huo Y, Qu Z, Rao Z. Investigation on the thermal behavior of Ni-rich NMC lithium ion battery for energy storage. Appl Therm Eng 2020;166:114749.
[57] Choudhari VG, Dhoble AS, Sathe TM. A review on effect of heat generation and various thermal management systems for lithium ion battery used for electric vehicle. J Energy Storage 2020;32:101729.
[58] Ngatchou P, Zarei A, El-Sharkawi A. Pareto multi objective optimization. In: Proceedings of the 13th international conference on, intelligent systems application to power systems. IEEE; 2005, p. 84–91.